A comprehensive combustion chemistry study of n-propylcyclohexane

Citation for the original published paper (version of record):
Ahmed, A., Corrubia, J., Al-Lehaibi, M. et al (2021). A comprehensive combustion chemistry study of n-propylcyclohexane. Combustion and Flame, 233.
http://dx.doi.org/10.1016/j.combustflame.2021.111576

Combustion and Flame 233 (2021) 111576

Contents lists available at ScienceDirect

Combustion and Flame

journal homepage: www.elsevier.com/locate/combustflame

A comprehensive combustion chemistry study of *n*-propylcyclohexane

Ahfaz Ahmed[a,b,*], Julius A. Corrubia[c], Moaz Al-Lehaibi[a,d], Farinaz Farid[c], Heng Wang[a], Zhandong Wang[a], Bingjie Chen[a], William L. Roberts[a], David L. Miller[c], Aamir Farooq[a], Nicholas P. Cernansky[c], S. Mani Sarathy[a,*]

[a] King Abdullah University of Science and Technology (KAUST), Clean Combustion Research Center, Physical Sciences and Engineering Division, Thuwal, 23955, Kingdom of Saudi Arabia
[b] Chalmers University of Technology, Department of Mechanics and Maritime Sciences, Division of Combustion and Propulsion Systems, Gothenburg, 41258, Sweden
[c] Drexel University, Department of Mechanical Engineering and Mechanics, Philadelphia, 19104, USA
[d] Umm Al-Qura University, Mechanical Engineering Department, College of Engineering and Islamic Architecture, Makkah, 24211, Kingdom of Saudi Arabia

ARTICLE INFO

Article history:
Received 29 December 2020
Revised 18 June 2021
Accepted 19 June 2021

Keywords:
Jet fuels
Alkylcyclohexane
Chemical kinetic modelling
Ignition
Speciation in flow reactor

ABSTRACT

Alkylated cycloalkanes are vital components in gasoline, aviation, and diesel fuels; however, their combustion chemistry has been less investigated compared to other hydrocarbon classes. In this work, the combustion kinetics of *n*-propylcyclohexane (*n*-Pch) was studied across a range of experiments including pressurized flow reactor (PFR), jet stirred reactor (JSR), shock tube (ST), and rapid compression machine (RCM). These experiments cover a wide range of conditions spanning low to intermediate to high temperatures, low to high pressures at lean to rich equivalence ratios. Stable intermediate species were measured in PFR over a temperature range of 550–850 K, pressure of 8.0 bar, equivalence ratio (φ) of 0.27, and constant residence time of 120 ms. The JSR was utilized to measure the speciation during oxidation of *n*-Pch at φ of 0.5–2.0, at atmospheric pressure, and across temperature range of 550–800 K. Ignition delay times (IDTs) for *n*-Pch were measured in the RCM and ST at temperatures ranging from 650 to 1200 K, at pressures of 20 and 40 bar, at $\varphi = 0.5,\ 1.0$. In addition, a comprehensive detailed chemical kinetic model was developed and validated against the measured experimental data. The new kinetic model, coupled with the breadth of data from various experiments, provides an improved understanding of *n*-Pch combustion.

1. Introduction

1.1. Background

The aviation industry consumes a substantial quantity of hydrocarbon-based jet fuel every year, which adds significantly to global carbon emissions, and since 2013 alone emissions from aviation operations have risen by 26% [1]. Reduction of these emissions is an ongoing exercise, and it relies on the refinement of existing propulsion technologies involving combustion engines and fuel blends.

Several measures are adopted to improve aviation engines' performance and fuel efficiency, such as enhancements in the design of the compressor, combustor, and fuel injection systems, valves etc. [2–4]. On the fuel side, blending of biofuels to jet fuels [3,5,6] and enhancing the understanding of jet fuel's base component combustion characteristics which is also the focus area of this work. Typical jet fuels are a complex mixture of hydrocarbons and contains ~21% alkylated cycloalkanes, by mass, by global average survey estimates [7]. These alkylated cycloalkanes include methylcyclohexane (MCH), ethylcyclohexane (ECH), *n*-propylcyclohexane (*n*-Pch), *n*-butylcyclohexane (*n*-Bch) etc. Studies focussing on MCH, ECH, and *n*-Bch are available in significant detail in literature elucidating their combustion properties and detailed kinetic model development. However, studies detailing *n*-Pch combustion are limited in number and scope, and they do not present comprehensive investigations as typically available in the literature for other cycloalkanes. In the next section, a detailed review of combustion studies of alkylated cycloalkanes is provided.

* Corresponding authors.
E-mail addresses: ahfaz@chalmers.se, ahfaz.ahmed@kaust.edu.sa (A. Ahmed), mani.sarathy@kaust.edu.sa (S.M. Sarathy).

https://doi.org/10.1016/j.combustflame.2021.111576

1.2. Literature survey

1.2.1. Methylcyclohexane (MCH)

Han et al. [8] measured ignition delay of MCH and n-hexane blends in a constant volume reactor similar to an ignition quality tester at 20 bar and 820–920 K. Also, the effect of fuel injection parameters on heat release rate and ignition delay time were investigated. In another study Hong et al. [9] measured ignition delay times of MCH and ECH in a shock tube at low pressures of 1.5 and 3.0 atm, temperatures of 1280–1480 K, and $\varphi = 0.5, 1.0$. Pitz and coworkers [10] reported ignition delay measurements of MCH in a rapid compression machine (RCM) at 10–20 bar, 650–1100 K for stoichiometric mixtures and also proposed a kinetic mechanism. Vanderover et al. [11] conducted ignition delay measurements for MCH in a shock tube at pressure range of 10.8-69.5 atm, temperature range of 881–1319 K, and $\varphi = 0.25, 0.5, 1.0$. Similarly, Vasu et al. [12] also measured ignition delay time of MCH in shock tube over a wide pressure range in a shock tube from 1 to 50 atm, 795–1560 K, $\varphi = 0.5$–2.0. Weber et al. [13] performed ignition delay measurements in an RCM at 50 bar, 690–900 K, $\varphi =$ 0.5–1.5. Humer et al. [14] measured flame extinction and autoignition of MCH and other fuels in a laminar non-premixed flow in the counterflow configuration. In addition, a reduced kinetic mechanism was proposed which adequately predicted the experimental data. In 2019, Bissoonauth et al. [15] conducted an oxidation and pyrolysis study in jet stirred reactor across an extensive range of pressures (1–50 bar) and temperatures (500–1100 K) at three different experimental facilities and measured the concentrations of intermediates and end products. Narayanaswamy et al. [16] developed a detailed kinetic mechanism in the low to high-temperature region and improved the model using experimental data from the literature. MCH has also been studied in a Cooperative Fuels Research (CFR) engine by Yang and coworkers [17] by varying the compression ratio from 4 to 15. These investigations were conducted at $\varphi = 0.25$ and two inlet temperatures 120 and 200 °C and exhaust gasses were analyzed and various conjugated alkenes and cyclic oxygenates were measured. Wang et al. [18] studied MCH pyrolysis using synchrotron vacuum ultraviolet photoionization mass spectrometry at the National Synchrotron Radiation Laboratory (NSRL), Hefei, China. Molecular-beam sampling was used to analyze the species formed during pyrolysis in a flow reactor. The authors also studied oxidation of MCH in premixed flames and several pyrolysis and flame intermediates were quantified. Orme et al. [19] studied oxidation and pyrolysis of MCH in a shock tube at experimental conditions of 1–4 bar, 1200–2100 K and $\varphi = 0.5$, 1.0, 2.0, and proposed a detailed kinetic model. In another work, a mechanism describing high temperature combustion of a range of n-alkanes up to n-dodecane and cyclohexane, and methyl-, ethyl-, n-propyl and n–butyl–cyclohexane was developed by Wang and coworkers as JetsurF 2.0 [20]. Wu et al. [21] measured laminar flame speeds of MCH at high pressure of 10 atm and temperature of 353 K and at range of equivalence ratios $\varphi = 0.7$–1.7.

1.2.2. Ethylcyclohexane (ECH)

Husson et al. [22] conducted a jet stirred reactor study at 1 atm, 500–1100 K, and $\varphi = 0.25, 1, 2$ measuring speciation during oxidation of ECH. More recently, a shock tube was used to measure ignition delay times for ECH and n-Pch at atmospheric pressure, $\varphi = 0.5, 1.0$, and 2.0, temperatures of 1110–1650 K, and with a fixed fuel concentration of 0.5% [23]. Ignition simulations were performed using three previously developed and published chemical kinetic mechanisms which yielded acceptable agreement with the shock tube measurements at the studied equivalence ratios. Tian et al. [24] studied the ignition of ECH in a shock tube at 1.1–10 atm, 1000–1700 K, and $\varphi = 0.5$–2.0. Wang et al. [25] studied pyrolysis of ECH in a flow reactor at atmospheric pressure across temperature range of 900–1100 K and quantified the products using gas chromatography and synchrotron vacuum ultraviolet photoionization mass spectrometry. Wang et al. [26] then further expanded their investigation by measuring species for both oxidation and pyrolysis of ECH at low pressures of 30, 150 and 760 Torr.

1.2.3. Propylcyclohexane (n-Pch)

Ignition of n-Pch has been studied in an RCM at lean conditions at 620-930 K, 4.5–13.4 bar, and $\varphi = 0.3, 0.4, 0.5$ by Crochet [27]. Dubois et al. [28] studied the ignition characteristics of *n*-Pch in a shock tube at 10–20 bar, at higher temperature range of 1250–1800 K, $\varphi = 0.2$–1.5, and flame speeds in constant volume spherical bomb at 1 bar, 403 K, $\varphi = 0.6$–1.75. In addition, they also assembled a kinetic mechanism. Guo et al. [29] formulated a high-temperature *n*-Pch mechanism using their inhouse code ReaxGen and compared it with data from shock tubes, laminar flames, jet stirred reactors from literature. Ristori et al. [30] measured speciation during oxidation of *n*-Pch in JSR at atmospheric pressure, 950–1250 K, $\varphi = 0.5$–1.5 and also developed a kinetic model. Farid [31] and Corrubia [32,33] at Drexel university measured *n*-Pch intermediate species in a Pressurized Flow Reactor (PFR) at 8 atm and a range of temperatures from 550 to 850 K. Pousse et al. [34] studied flame structures of methane flames doped with *n*-PCH and also proposed a kinetic model for *n*-Pch combustion.

1.2.4. Butylcyclohexane (n-Bch)

Oxidation of blends of n-Bch and heptane has been studied in both a shock tube and rapid compression machine by Conroy [35]. The ignition delay time measurements were made at 1–50 atm, 580–1550 K, and $\varphi = 0.3, 0.5, 1.0$ and 2.0. In another study, Mao et al. [36] conducted an extensive RCM investigation of *n*-Bch ignition characteristics at 10, 15, 20 bar; 612–1374 K and $\varphi = 0.5, 1.0$, 1.5. The oxidation of *n*-Bch was studied in PFR [37, 38] with an initial fuel molar fraction of 1082 ppm ($\varphi = 0.38$), the temperature of 600–820 K, pressure of 8 atm, and residence time of 120 ms. Detailed intermediate speciation with a GC / MS revealed straight-chain species (i.e. alkenes and aldehydes) and various cyclic compounds (i.e., cycloalkenes, ketone-substituted cycloalkanes and several two ring cyclic structures). The work from Drexel also developed a semi-detailed *n*-Bch low-temperature oxidation mechanism that captured the measured PFR reactivity trends which were characterized by low temperature increasing reactivity and NTC behavior decreasing overall reactivity.

An experimental and modelling study using shock tubes and a rapid compression machine was performed with *n*-Bch by Pitz and coworkers [39] at temperatures of 630–1420 K, pressures of 10, 30, 50 atm and $\varphi = 0.3, 0.5, 1.0, 2.0$. In addition, a detailed *n*-Bch chemical kinetic model was developed to simulate its ignition at both low and high temperatures. The experimental ignition delay times were used to improve the chemical kinetic model. The authors concluded that rate constant parameters developed from recent ab initio calculations provided better predictions of experimental ignition delay time data than the estimated rate constant parameters based on analogies to other molecules [40]. Recently, Zhang and coworkers [41] conducted experimental ignition delay measurement of *n*-Bch in shock tube at 2, 5, 15 atm; 707–1458 K; $\varphi = 0.5, 1.0, 2.0$. Mao and coworkers [36,42] conducted studies on *n*-Bch using rapid compression machine and shock tube measuring ignition delay at 10–20 bar, 612–1374 K, $\varphi = 1.0, 1.5$ and speciation during oxidation in flow reactor 1 bar, 650–1075 K, $\varphi = 1.0$, 1.5. In addition, they also proposed a detailed kinetic mechanism. Hong et al. [9] compared ignition delay of cyclohexane, MCH, and *n*-Bch at 1.5, 3 bar, 1280–1480 K, $\varphi = 0.5, 1.0$. Ali et al. [43] studied thermal decomposition of *n*-Bch at 0.01–1 atm, 800–2100 K. Liu et al. [44] studied ignition of various cyclohexanes including n-Bch in counterflow burner at 1 bar and 373 K.

It is evident from the literature review that *n*-Pch warrants further combustion investigation, especially at low to intermediate temperatures and higher pressures. Besides, previous studies have not proposed a detailed chemical kinetic model for *n*-Pch combustion for wide range of pressures, temperature and equivalence ratios elucidating ignition and speciation characteristics.

To this end, this work presents a detailed examination of combustion chemistry of *n*-Pch wherein ignition delay time (IDT) measurements have been made at low to high pressures in RCM and shock tube (ST). Intermediate speciation studies were conducted in a jet stirred reactor (JSR) and pressurized flow reactor (PFR) experiments. Further, a detailed chemical kinetic model has been proposed and validated against the acquired experimental dataset.

The experimental measurements in the JSR, ST, and RCM were conducted at King Abdullah University of Science and Technology (KAUST). The JSR facility at KAUST was utilized to measure speciation during oxidation of *n*-Pch at φ = 0.5, 1.0, 2.0, atmospheric pressure, and in the temperature range of 550–800 K. IDT's of *n*-Pch mixtures were measured in an RCM and ST for low to high temperatures ranging from 650-1200 K, at higher pressures of 20 and 40 bar, and $\varphi = 0.5,\ 1.0$. Speciation measurements were conducted in PFR facility at Drexel University in the temperature range of 550–850 K and pressure of 8.0 atm. A detailed chemical kinetic model for *n*-Pch was developed to describe ignition characteristics, fuel consumption pathways and product species formation. Comparisons between results computed with the developed model and the measured experimental data are presented, and the kinetics of *n*-Pch combustion are discussed.

2. Chemical kinetic modeling

This section discusses the chemical kinetic model of *n*-Pch proposed in this work which is consistent with earlier works of Wang et al. investigating flame and pyrolysis kinetics of MCH [18] and ECH [26]. The developed mechanism has 1442 species and 6397 reactions, and the base C_0–C_4 chemistry is described by Aramcomech 2.0 [45].

In the following section, details of important reaction classes in the low-temperature and high-temperature mechanism and the estimation of thermochemistry and kinetic rate parameters are discussed.

2.1. High-Temperature reactions

2.1.1. Unimolecular reactions of n-Pch

The uni-molecular reactions of *n*-Pch include three dissociation and seven isomerization pathways, as shown in Fig. 1. As in Wang's ethylcyclohexane mechanism [26], H elimination reactions are not included due to their higher activation energies than competing decomposition and isomerization channels [26]. The rates for these reactions were assigned based on analogous pathways from the ethylcyclohexane mechanism [26], which in turn, were calculated by Zhang et al. [46] using RRKM/master equations. The uni-molecular decomposition leads to the formation of ethylcyclohexyl, methylcyclohexyl and cyclohexyl radicals which further undergo β-scission to produce alkenyl and alkyl species. Specifically the rates of pathways leading to methyl- and ethylcyclohexyl radicals were adopted from analogous pathways of n-butane combustion from Oehlschlaeger et al. [47]. The isomerization channels lead to the formation of various straight and branched C-9 alkenes, which are subsequently consumed through H-atom abstraction and β-scission channels to smaller species.

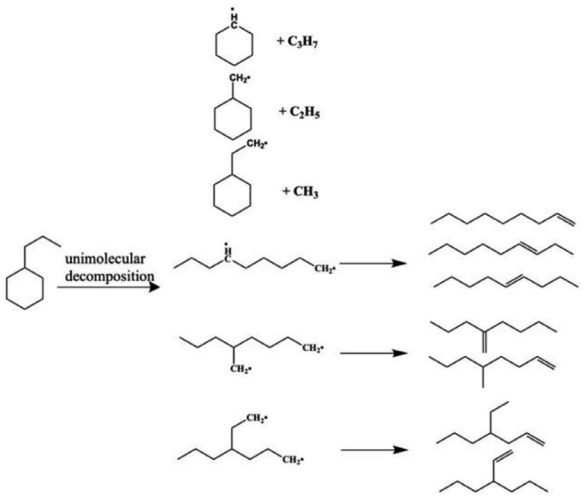

Fig. 1. Unimolecular reactions of n-propylcyclohexane.

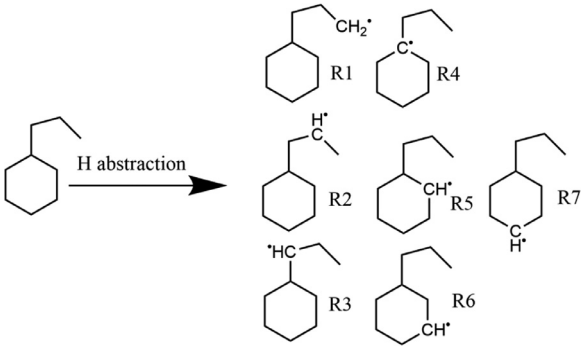

Fig. 2. n-propylcyclohexane radicals produced after H-atom abstraction from various sites.

2.2. Hydrogen abstraction reactions

Hydrogen abstraction from the fuel molecule is an essential class of reactions responsible for fuel consumption. In the mechanism, *n*-Pch undergoes initial H-atom abstraction by various species (e.g., O_2, O, OH, HO_2, H, CH_3), leading to the production of seven distinct fuel radicals as shown in Fig. 2. The majority of H-atom abstraction rates by different species leading to fuel radicals R1, R2 and R3 were adopted from JetsurF 2.0 [20]. In addition, some rates from literature were also used at these sites (R1, R2, R3) to improve the performance of the model. Specifically, abstraction by OH radical at sites R2 and R3 were adopted from experimentally measured rates from Badra et al. [48] and abstraction by H radical at site R2 was adopted from Liu et al. [49]. The rates from Badra et al. [48] were tuned within 60% of published rates while the rate from Liu et al. [49] was increased by a factor of 2. The rate of H atom abstractions by radicals O, H, CH_3, O_2, HO_2 from the sites on the ring (R4, R5, R6, R7) were adopted from Wang's ECH work [26] where the rates of abstraction by H radical were increased by a factor of 2. Rate of attack by OH on the secondary sites of the ring (R5, R6, R7) were adopted from Weber et al. [13] and were also tuned within a factor of 2, while the rate for site R4 was adopted from Wang et al.[18,26].

There is still lack of reliable theoretical and experimental reaction rate data for *n*-Pch combustion and hence modifications are needed before rates from analogous compounds could be adopted. In this case, reaction rates were tuned to improve ignition prediction of the mechanism in the intermediate and high temperature

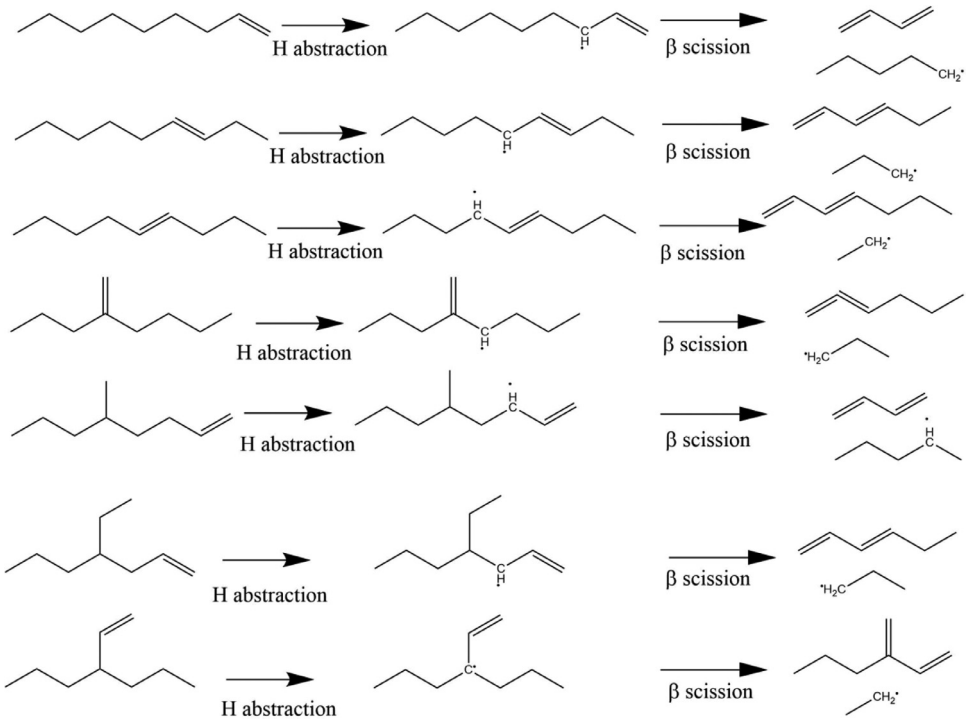

Fig. 3. Consumption of alkenes produced via unimolecular reactions of n-propylcyclohexane.

region and the tuned reactions were identified by conducting sensitivity analysis.

The alkyl radicals produced were consumed through β-scission reactions leading to the formation of alkenes and alkenyl species.

2.3. Consumption of alkanes and alkenes

Unimolecular reactions of *n*-Pch leads to formation of seven linear and branched alkenes (Fig. 1). These alkenes are then consumed through allylic H-atom abstraction reactions followed by β-scission leading to formation of miscellaneous species and di-enes. These di-enes are further consumed by H-atom abstraction reactions and β-scission reactions to produce smaller species already present in the base mechanism or the mechanism of ECH [26]. The reaction rates of allylic H-atom abstraction and β-scission reactions were adopted from Wang et al. [18,50]. These consumption pathways are exhibited in Fig. 3 for various H-atom abstraction and β-scission pathways. Due to relatively higher activation energy barrier of these reactions, these species are expected to be formed in minor quantities hence a simplified consumption scheme by allylic H-atom abstraction is considered, however this simplification could be revisited when more accurate rates are available for production of these species.

Another set of alkenyl and alkyl species along with alkenes are produced via β-scission of fuel radicals which include ring-opening pathways. They undergo β-scission to smaller alkenes, as shown in Fig. 4. The rates for these β-scission reactions were adopted from different alkanes and alkene species with the analogous position of the double bond, chain length and radical sites from Wang et al. [26].

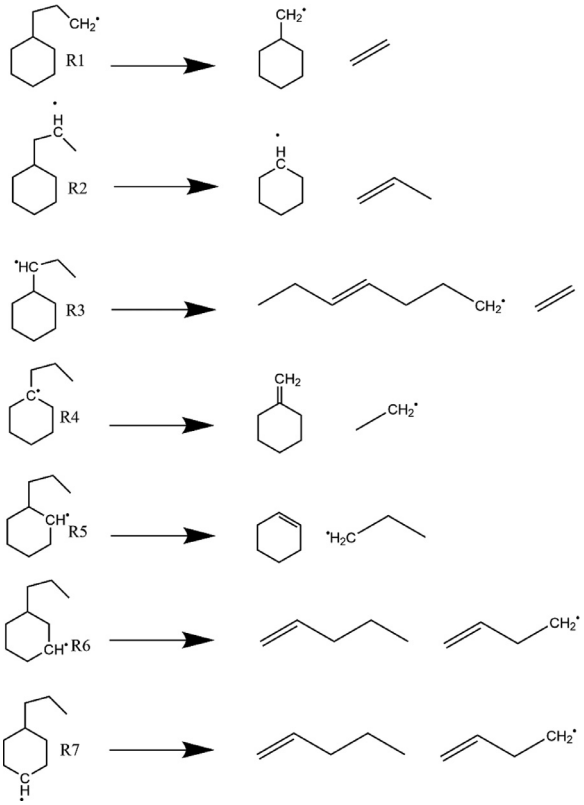

Fig. 4. Alkenyl radical decomposition of n-propylcyclohexyl radical.

2.4. Low-Temperature mechanism

The first step in low-temperature oxidation chemistry is the addition of the oxygen molecule (O_2) to the fuel radicals (R1-R7) leading to the formation of seven alkylperoxy radicals (RO_2), as shown in Fig. 5 for R6. The reaction rates for these steps have been adopted based on Curran et al. [51], which are originally based on works of Lenhardt et al. [52] and Atkinson et al. [53] for the propyl branch while the rates on the ring are from Fernandes et al. [54]. The next major step in the low-temperature chain branching step is the isomerization of alkylperoxy radicals (RO_2) to hydroperoxy

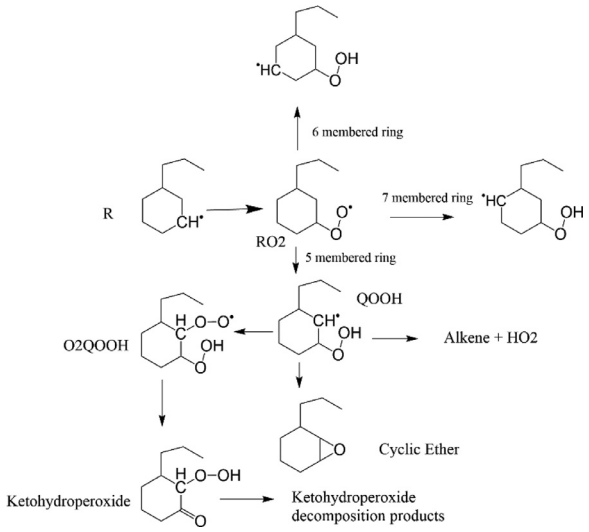

Fig. 5. Low-Temperature branching pathways for n-Pch.

alkyl radicals (QOOH). These reactions proceed via an internal H-atom transfer via 5, 6, 7 and 8 membered transition state rings. Fig. 5 depicts this pathway with a five, six and seven-membered transition state. The rates for this class of reactions were based on analogies for alkanes by Sarathy et al. [40], which are based initially on the work of Curran et al. [51]. The internal H-atom transfer leads to creating a carbon centered radical, which undergoes second O_2 molecule addition, leading to hydroperoxy alkylperoxy radicals (O_2QOOH). These reaction rates are adopted from Lenhardt et al. [52] and Curran et al. [51]. There are other competing pathways leading to the formation of alkenes and cyclic ethers leading to accumulation of relatively stable species hence making the chemical system less reactive. The rates for these reactions were adopted from Curran et al. [51].

Recently some studies have also demonstrated pathways leading to addition of third O_2 [55,56] molecule to P(OOH)$_2$ which is produced by intramolecular isomerization of O_2QOOH. These pathways are shown to have significant impact on low temperature reactivity of long chain alkanes but at present we do not have reliable rate constants to include such pathways in the mechanism.

The hydroperoxy alkylperoxy radicals isomerizes to form ketohydroperoxides (carbonyl hydroperoxide), and the rates are adopted from Curran et al. [51,57]. The last step in the low-temperature branching pathway is the decomposition of ketohydroperoxide producing sets of radicals and stable species. These reactions are assigned as irreversible and forward rates have been adopted from Sarathy et al. [40]. There are multiple other classes of reactions in the low-temperature oxidation scheme involving chain propagation and termination steps, and the rates have been adopted by analogous sites and structures from Sarathy et al. [40].

In addition to a detailed description of the chemistry of *n*-Pch in the low and high-temperature region, this mechanism also includes the oxidation pathways leading up to *n*-propylbenzene and its consumption as proposed by Darcy et al. [58].

2.5. Thermochemistry

The thermochemistry for multi-ring species was calculated in this work using quantum chemical methods with the Gaussian 09 [59] suite of programs. During these calculations, merged ring structures are optimized with B3LYP/6–31+*G*(d,p) [60,61] level of theory, and then the total energies are determined with CBS-QB3 [62]. Entropy and heat capacity contributions as a function of temperature are then determined using moments of inertia, vibration frequencies, symmetry, electron degeneracy, number of optical isomers and the known mass of each species. SMCPS [63] program is applied to calculate the contributions of translation, external rotation, and vibrations by using standard formulas from statistical mechanics. Vibrational frequencies are scaled by a factor of 0.964 [64] to calculate standard entropy and heat capacity at the B3LYP/6–31+*G*(d,p) level of calculation. Rotator [65] program is used to calculate the contribution from the corresponding internal rotor torsion frequencies. In this work, a t*e*n-parameter Fourier series function is used as a torsional potential curve to estimate free internal rotation contribution. The species for which thermochemistry has been calculated are shown in Fig. 6, and detailed function and parameters are shown in the supporting material. Thermochemistry for simpler species has been calculated with Benson's group additivity approach [66] using THERM software [67] as implemented on CloudFlame [68].

3. Experimental measurements and methodology

3.1. Pressurized Flow Reactor(PFR)

The Drexel University Pressurized Flow Reactor (PFR) used in this study is a turbulent flow reactor designed to study the low to intermediate temperature oxidation of hydrocarbons, shown schematically in Fig. 7. The design achieves reduced gradients in temperature and the flow field to allow the use of plug flow assumptions [69,70] for data analysis and modelling. The PFR contains a 22.5 mm ID, 40 cm long quartz reactor tube to provide an environment where surface reactions are negligible within a stainless steel pressure vessel rated to a maximum of 20 bar; however, 8 bar was selected for this study to allow comparison to the work of Natelson et al. [38]. The annular volume between the quartz reactor tube and the pressure vessel is at the same pressure as the reaction chamber. During a typical oxidation experiment, the oxidizer stream (composed of high purity nitrogen (purity = 99.9%) and high purity oxygen (purity = 99.994%)) is mixed with high-pressure pre-vaporized fuel/nitrogen in an opposed jet annular mixing nozzle at the inlet to the quartz reactor tube. For the maximum as designed PFR operating conditions (<1000 K, <20 bar), a nominal mixing time was calculated to be 1.25 ms [69] A water-cooled, borosilicate glass-lined stainless-steel sample probe extracts and quenches samples from the centerline of the quartz reactor tube.

A direct transfer controlled cool down (DT-CCD) operational procedure was used to minimize the time between sample collection and analysis of stable intermediate species in the gas chromatograph (GC) / mass spectrometer (MS) / flame ionization detector (FID). The DT-CCD method developed by Kurman et al. [71] produced a carbon balance of 90% at 550–850 K.

During an oxidation experiment, the PFR was heated to the maximum desired reaction temperature of approximately 850 K when a syringe pump injected fuel into a 300 °C nitrogen stream that ensured complete fuel vaporization. The fully vaporized fuel/nitrogen mixture rapidly mixed with the oxidizer stream in an opposed jet annular mixing nozzle, with a nominal mixing time of 1.25 ms. The PFR experiment flow rates were: 0.750 ml/min *n*-Pch, 8.40 slpm O_2, 161.2 slpm N_2 for the oxidizer stream, plus 20.00 slpm N_2 for *n*-Pch fuel vaporization. The relatively large nitrogen bulk flow rate acted as a diluent to limit the temperature rise due to heat release to a maximum of approximately 10 K at maximum reactivity as measured from the mixing nozzle to the sample probe. After the system stabilized, the sample probe was positioned for a reaction time of 120 ms, and the first sample was withdrawn for analysis. Stable intermediate species in the sample were identified and quantified with the GC/MS/FID and CO/CO_2/O_2 detector. During the analysis time for the first sample, the PFR

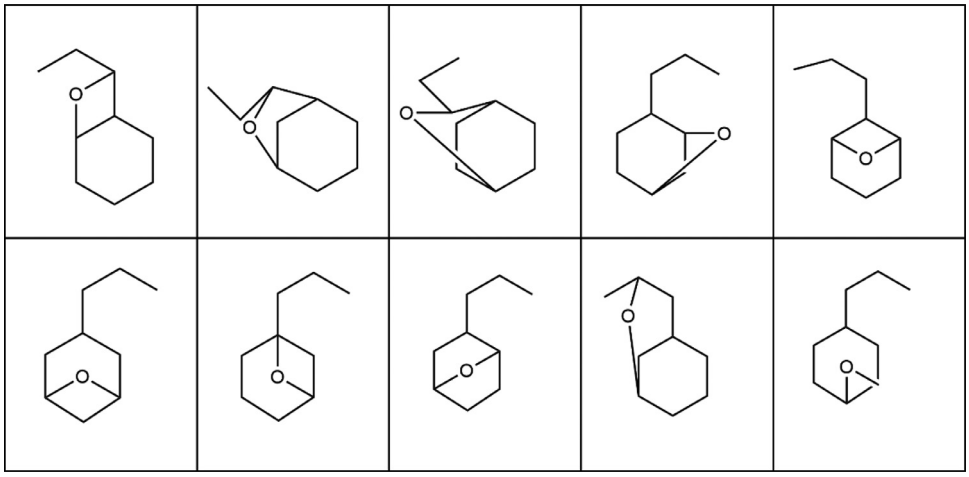

Fig. 6. List of species for which thermochemistry data has been calculated in this work using quantum chemistry approach.

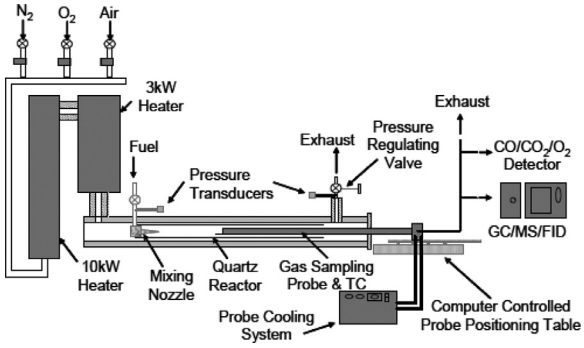

Fig. 7. Schematic of the Drexel Pressurized Flow Reactor facility.

temperature was gradually reduced to the next selected sample temperature. The probe was repositioned to maintain the constant reaction time of 120 ms. This procedure was repeated for all collected samples.

3.2. Jet Stirred Reactor(JSR)

The oxidation of *n*-Pch was studied in a jet stirred reactor (JSR) at KAUST. Species profiles for *n*-Pch and intermediates (CO, C_2H_4, C_3H_6) were analyzed at atmospheric pressure at a range of temperatures (500–800 K) and equivalence ratios (φ = 0.5, 1.0, 2.0). The JSR experimental setup consists of a 76 cm^3 spherical quartz reactor with four nozzles of 0.3 mm diameter to attain homogeneity of species and temperature distribution. The JSR is connected to upstream and downstream quartz tubes of diameter 25.4 mm. *n*-Pch was stored in a 10 ml syringe and was injected using a syringe pump at a constant flow rate. After vaporization, fuel was diluted with N_2 and mixed with O_2 at the JSR entrance, and the flow rate was regulated with a multi-gas controller (MKS) mass flow meter. The reactor and part of the upstream and downstream quartz tubes were symmetrically placed in an electrical heating furnace to promote oxidation reactions. The furnace temperature was monitored via a K-type thermocouple inserted into a quartz shield [72]. The quartz tubes (upstream and downstream) located outside the furnace were heated with electrical heating tape and maintained at 393 K using stainless-steel K-type thermocouples and temperature controllers.

Stable intermediates and fuel and oxidizer species were sampled by a sonic probe connected to the vacuum suction pump to prevent further reactions. All downstream tubing was heated to 373 K to avoid condensation. Gas composition was analyzed using a refinery gas analyzer (RGA), a uniquely designed gas chromatography system, coupling a flame ionization detector (FID) and a thermal conductivity detector (TCD) where helium was used as carrier gas. Capillary columns (Molecular Sieve 5A, 2 ft and 4 ft Unibeads 1S, HP-Al/S and DB-1) were used for species quantification including *n*-Pch, ethene, oxygen, carbon monoxide, carbon dioxide, and propene. The uncertainty in the measurement of fuel/oxygen concentration and intermediates is 10% and 20%, respectively. The uncertainty in temperature measurement is +/- 25 K. O_2 and N_2 gasses used during the experiments had purity over 99.99%. The JSR residence time was set to two seconds at atmospheric pressure. Further details about measurement methods and the apparatus are provided in [73]

3.3. Shock tube and rapid compression machine

High-pressure ignition delay time measurements of *n*-Pch were conducted using the shock tube and rapid compression machine facilities at KAUST. IDT measurements were performed over a wide range of experimental conditions, spanning the temperature range of 625 to 1100 K at two pressures, 20 and 40 bar and two equivalence ratios, 0.5 and 1. The shock tube (ST) and rapid compression machine (RCM) facilities at KAUST have been extensively reported in the literature [74, 75] and hence only a brief description is provided here.

The ST employed in this study consists of double diaphragm mid-section configuration, which allows improved control of the diaphragm burst pressure and higher control of the thermodynamic conditions behind the reflected shock wave. The shock tube is constructed with stainless steel and consists of two sections, namely driver and driven sections of similar length (6.6 m) and diameter (10 cm). The shock tube and mixing tank, along-with the mixing manifold, were heated to 100 °C to avoid any condensation of fuel on the inner walls. Near the end-wall of the driven section, six dynamic pressure transducers were installed to measure the incident shock speed. The measured shock speed and the *n*-Pch/oxidizer mixture's thermodynamic properties were utilized to calculate reflected shock temperature and pressure using one-dimensional shock jump equations. During the measurements, ignition delay time was computed using pressure signal and OH* chemiluminescence measurements through the sidewall and end-wall ports. Estimated uncertainty in the reflected shock temperature/pressure is <1% and the estimated uncertainty in the ignition delay times is ~ 20%. Gradual pressure rise behind the reflected shock wave, *dp/dt*, was measured to be 3% / ms; there-

Table 1
Experimental conditions for n-Pch oxidation studies in Pressurized Flow Reactor.

Parameter	Exp 1	Exp 2	Average	Uncertainty
n-Pch (ppm)	830	821	826	±20
O_2 (ppm)	42,100	42,100	42,100	± 1250
N_2 (ppm)	Balance	Balance	Balance	–
Equivalence Ratio, ϕ	0.27	0.27	0.27	± 0.05
Temperature (K)	550–850	550–850	550–850	± 5.0
Pressure (atm)	8.000	8.000	8.000	± 0.025
Residence Time (ms)	120	120	120	± 1.0

fore, a 3% *dp/dt* was imposed on zero-dimensional kinetic simulations [26].

The RCM facility at KAUST is equipped with a twin-opposed piston design that facilitates a higher degree of mechanical balance and shorter compression time than a single-piston configuration. The reaction chamber is 50.8 mm in diameter and stroke length of 169 mm per piston, allowing a compression ratio of 16.8:1. The pistons are equipped with a fast pneumatic compression system that helps achieve compression times (final 50% of compression stroke) of ~ 3 ms. The compressed gasses pressure was monitored using a pressure transducer (Kistler 6045) mounted on the combustion chamber during the compression and ignition process. To avoid forming roll-up vortices inside the core of the reaction chamber, creviced pistons with ~ 10% of the post-compression volume were employed [27]. Post compression heat loss from the RCM was accounted for by using non-reactive volume profiles [28] during chemical kinetic simulations. Estimated uncertainty in the RCM ignition delay measurements is ~ 15%. The purity of gasses used during these measurements are CO_2: 99.995%, N2: 99.995%, O2:99.995% with traces of Ar (<1 ppm), N2 (<1 ppm), Moisture (<2 ppm). Non-reactive RCM volume profiles required for simulations and mixture fractions are provided as Supplementary Material.

4. Results and discussion

4.1. Pressurized Flow Reactor(PFR): experimental and modelling

Oxidation of *n*-Pch was studied in the Drexel PFR at two nearly identical experimental conditions, as shown in Table 1. The results are the average of both experiments with the uncertainties being ±1 standard deviation for stable intermediates measured with the GC/MS/FID, and equal to the equipment uncertainty for carbon monoxide, carbon dioxide, and oxygen.

During the PFR study (i.e., <850 K), carbon monoxide formation is an indicator of low-temperature oxidation reactivity as there is little conversion of CO to CO_2 [76] at low temperatures. Fig. 8 presents a reactivity map with the molar fractions of carbon monoxide, carbon dioxide, molecular oxygen, and *n*-Pch plotted concerning temperature. The oxidation behavior of *n*-Pch exhibits classical NTC behavior. The start of NTC for *n*-Pch, as indicated by the temperature at which the molar fraction of CO peaks and begins to decrease, occurs at approximately 700 K with CO production of roughly 770 ppm. Also, carbon dioxide levels at NTC start is about 180 ppm, which is similar to previous PFR experiments performed on straight-chain alkanes such as *n*-decane and *n*-dodecane [70,77], as well as the previously studied methyl-alkylated alkane, 2,7-DMO [31]. Namely, the carbon dioxide profile tracks the carbon monoxide profile over the low to intermediate temperature regime, but at lower levels on the order of 25%–35% of the CO molar fraction. Lastly, at NTC start where maximum reactivity exists corresponds to a minimum in the *n*-Pch and molecular oxygen molar fraction profile. At NTC start, the *n*-Pch molar fraction is approximately 115 ppm which translates to 86% fuel conversion. The O_2 molar fraction is about 40,000 ppm which corresponds to approximately 5% of the reactant O_2 being consumed suggesting that C–H remains in fuel fragments.

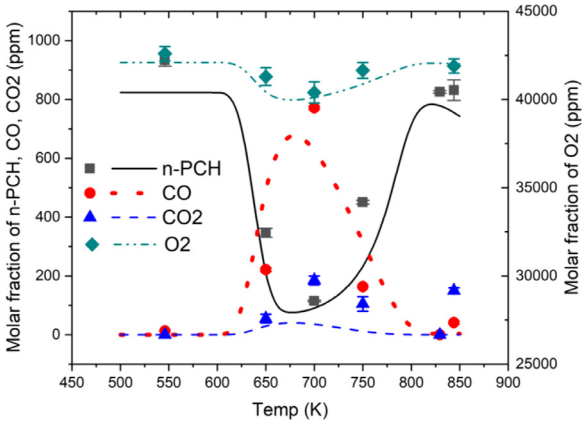

Fig. 8. Pressurized flow reactor simulations: Species profile from experiment and Chemkin pro simulations for n-Pch, O2, CO, CO2.

These trends are like those observed in the related *n*-Bch oxidation study [38] as shown in Fig. 3 in [38]. Both *n*-Pch and *n*-Bch studies were for 8 bar pressure, 550–850 K, 120 ms residence time, but different fuel loading as discussed below. The NTC start temperature for *n*-Pch shifted approximately 20 °C higher than *n*-Bch. The trend follows results observed by Kurman et al. [77], in which NTC start occurred at 675 K for *n*-dodecane, and NTC start occurred at 695 K *n*-decane. This illustrates the general observation that NTC start for smaller and simpler chemical structures (e.g., *n*-Pch, and *n*-decane) occurs at higher temperatures as compared to larger and more complex chemical structures (e.g., *n*-bch, and *n*-dodecane) for low to intermediate temperature regime oxidation. Also, the peak CO level for *n*-Pch was roughly 800 ppm at approximately 690 K and around 1600 ppm at approximately 670 K for *n*-Bch. This translates to about 11% of the *n*-Pch fuel carbon converting to produce CO at approximately 690 K (i.e., NTC start temperature for *n*-Pch) and about 14% of the *n*-Bch fuel carbon converting to produce CO at around 670 K (i.e., NTC start temperature for *n*-Bch). This indicates peak CO levels are highly dependent on initial fuel loading since *n*-Pch was initially 826 ppm and *n*-Bch was initially 1082 ppm. For comparing different fuels' reactivity at other fuel loading conditions, the NTC start temperature is suggested as a fuel reactivity indicator since it is strongly dependent on the oxidation chemistry of a particular fuel rather than fuel loading.

During these experiments seventy-seven stable intermediate species were identified and quantified using the GC/MS/FID system and $CO/CO_2/O_2$ detector during both *n*-Pch experiments. The carbon balances for all sample temperatures were greater than 90%. The minimum occurring at 700 K. Supplementary material lists the sixty-two stable intermediate species measured at molar fractions greater than approximately one ppm and their corresponding uncertainties. The fifteen stable intermediate species measured at molar fractions less than approximately 1 ppm included: 1-hexene; *n*-butylcyclohexane; 1,3-pentadiene; 2-butene; 2-methylcyclohexyl propionate; cyclohexene, 4–butyl; cyclohexene, 1–butyl; cyclohexanol, 3-methyl-2-(1-methylethyl)- (1a,2a,3a); cis-7-dece*n*-1-al; cyclohexanone, 2-(2-butynyl)-; 1,3-isobenzofurandione, hexahydro-, trans-; 2,2-bifuran, octahydro-; cyclohexanone, 2–butyl; 2-(4-methylcyclohexylidene)–1-propanol; 9-Ethylbicyclo(3.3.1)nona*n*-9-ol. The entire list of species quantified during these experiments is included in the supplementary material.

Another observation in PFR measurements is mismatch of fuel concentrations between 550 K and 850 K. The Pressurized Flow Re-

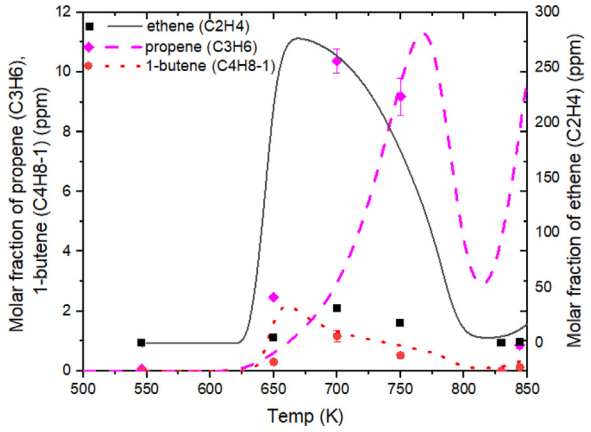

Fig. 9. Pressurized flow reactor simulations: Species profile from experiment and Chemkin pro simulations for ethene propene, 1-butene.

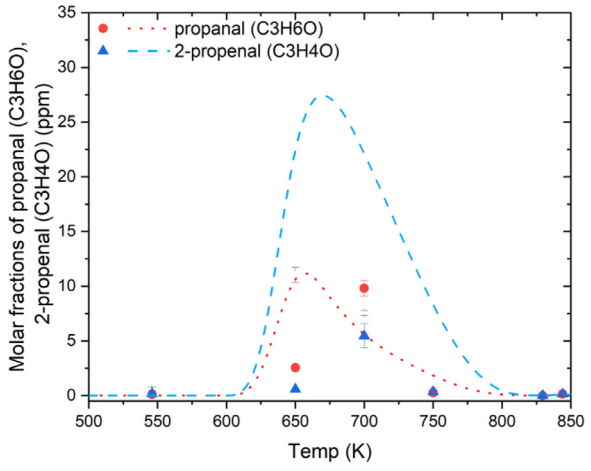

Fig. 10. Pressurized flow reactor simulations: Species profile from experiment and Chemkin pro simulations for aldehydes: propanal and 2-propenal.

actor (PFR) experiment begins at the higher temperature of 850 K and is reduced to the lower temperature of 550 K over time at approximately 50 K increments. The reason for less fuel recovered at the lower temperatures is likely due to the gas chromatograph/mass spectrometer (GC/MS) drift over time.

Chemical kinetic simulations for PFR oxidation were carried out with the kinetic model developed in this study using Chemkin Pro-ver. 19.2 [78]. The energy equation was solved for the plug flow reactor model with single inlet and outlet stream under adiabatic conditions using the reactor geometry, experimental conditions and initial species concentration to simulate the experiments accurately. In Fig. 8, we compare experimental and simulation species profiles for *n*-Pch, O_2, CO and CO_2. The simulated reactivity profile of *n*-Pch simulations closely predicts the consumption of *n*-Pch across the entire measurement range except for over prediction of fuel consumption in the NTC region. Consistent with higher predicted fuel consumption in the NTC region, the O_2 profile also shows higher consumption in the NTC region. The model predicts higher CO before, and in the NTC region, however, the predicted concentration of CO is lower at the start of NTC.

In Fig. 9, experiment and simulation results of various alkene intermediates produced during oxidation of *n*-PCH are presented. During the oxidation process, short chain alkenes observed are i.e. ethene, propene and 1-butene and no larger alkene concentrations were measured.

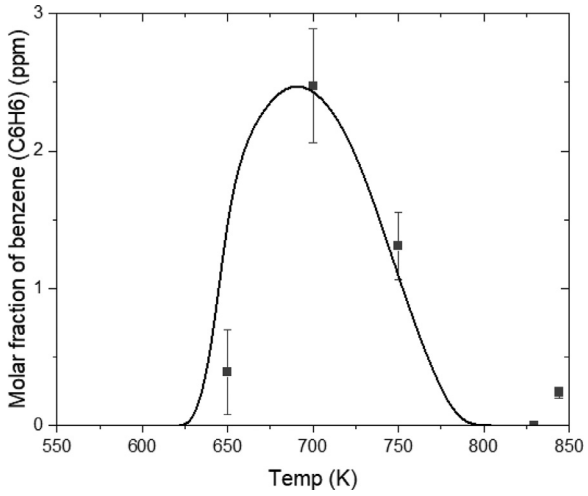

Fig. 11. Pressurized flow reactor simulations: species profiles from experiment and simulations for aromatics: benzene.

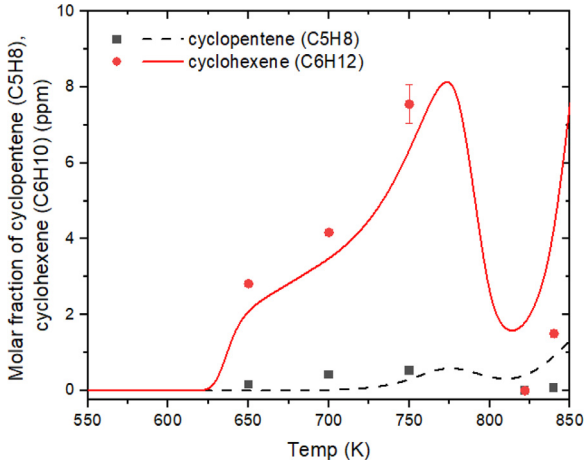

Fig. 12. Pressurized flow reactor simulations: Species profile from experiment and Chemkin pro simulations for cyclic alkenes: cyclopentene and cyclohexene.

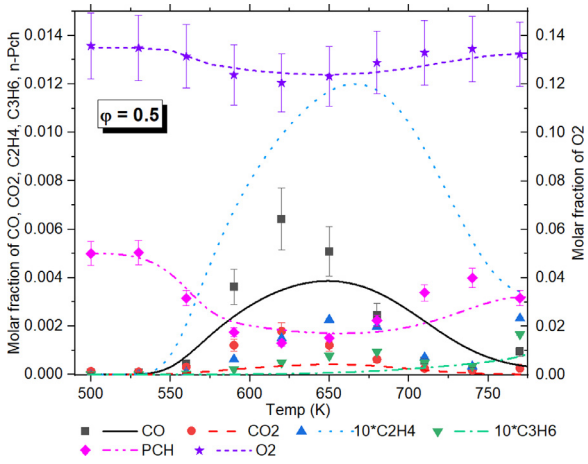

Fig. 13. Jet stirred reactor simulations: species profiles from experiment and simulations for n-Pch, O2, C2H4, C3H6, CO, CO2 at $\varphi = 0.5$. (For interpretation of the references to colour in this figure legend, the reader is referred to the web version of this article.)

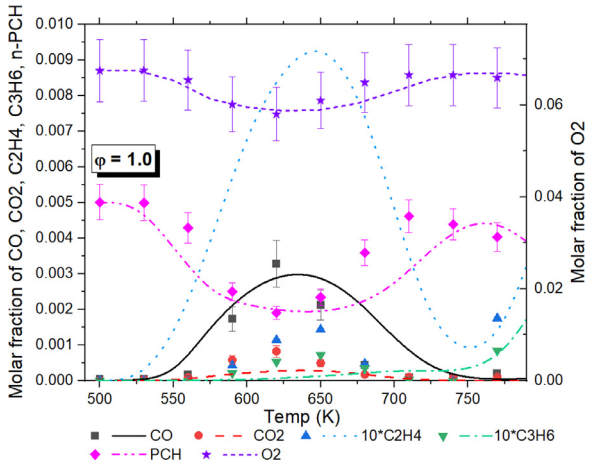

Fig. 14. Jet stirred reactor simulations: species profiles from experiment and simulations for n-Pch, O2, C2H4, C3H6, CO, CO2 at $\varphi = 1.0$. (For interpretation of the references to colour in this figure legend, the reader is referred to the web version of this article.)

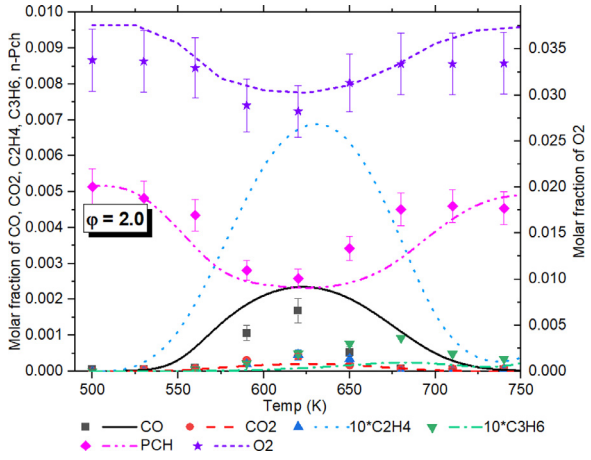

Fig. 15. Jet stirred reactor simulations: species profiles from experiment and simulations for n-Pch, O2, C2H4, C3H6, CO, CO2 at $\varphi = 2.0$. (For interpretation of the references to colour in this figure legend, the reader is referred to the web version of this article.)

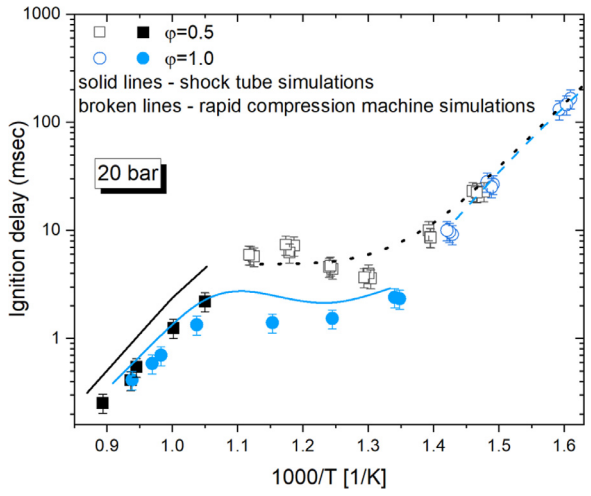

Fig. 16. Comparison of ignition delay experiments and simulations in shock tube and rapid compression machine at 20 bar.

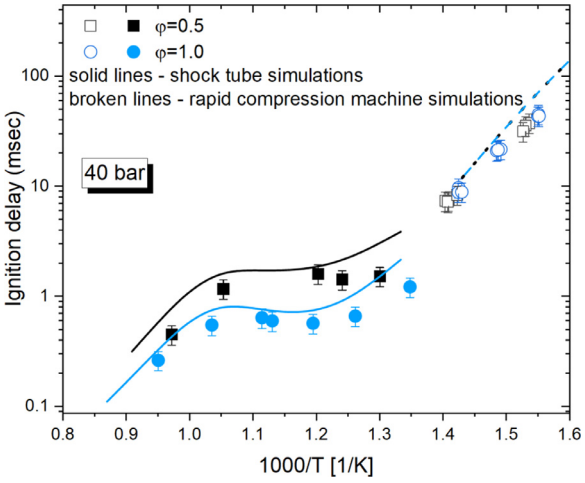

Fig. 17. Comparison of ignition delay experiments and simulations in the shock tube and rapid compression machine at 40 bar.

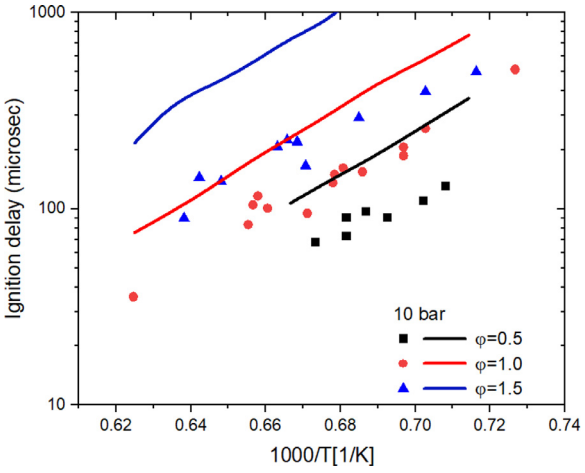

Fig. 18. Comparison of experimental data from Dubois et al. [28] and the ignition delay predictions using the n-Pch kinetic model proposed in this study. (For interpretation of the references to colour in this figure legend, the reader is referred to the web version of this article.)

The computed species profile of propene captures the experimental trend and the overall peak concentration produced; however, it shows a shift towards high temperature, resulting in lower production rates before the NTC region. Also, towards the high temperature end, the concentration of propene is overpredicted. 1-Butene was observed in low concentrations which is well predicted by the model except at 650 K. The concentration of ethene is largely over predicted in the intermediate temperature regime. The concentrations of these alkenes produced is minor compared to significant intermediates and products (i.e., CO, CO_2) and are not expected to have any significant effect on combustion characteristics of *n*-Pch, so the kinetic model was not tuned further to improve their prediction.

The developed kinetic scheme also considers production and consumption of smaller aldehydes during the oxidation of *n*-Pch. Several aldehydes were measured, including acetaldehyde, propanal, 2-propenal, butanal, and 1,3,5-trioxane. However, the kinetic model only includes propanal and 2-propenal production and consumption pathways. As shown in Fig. 10, the computed concentrations of propanal overpredict PFR measurements in the low-temperature regime and underpredict the PFR measurements at NTC start. The computed species profile of 2-propenal cap-

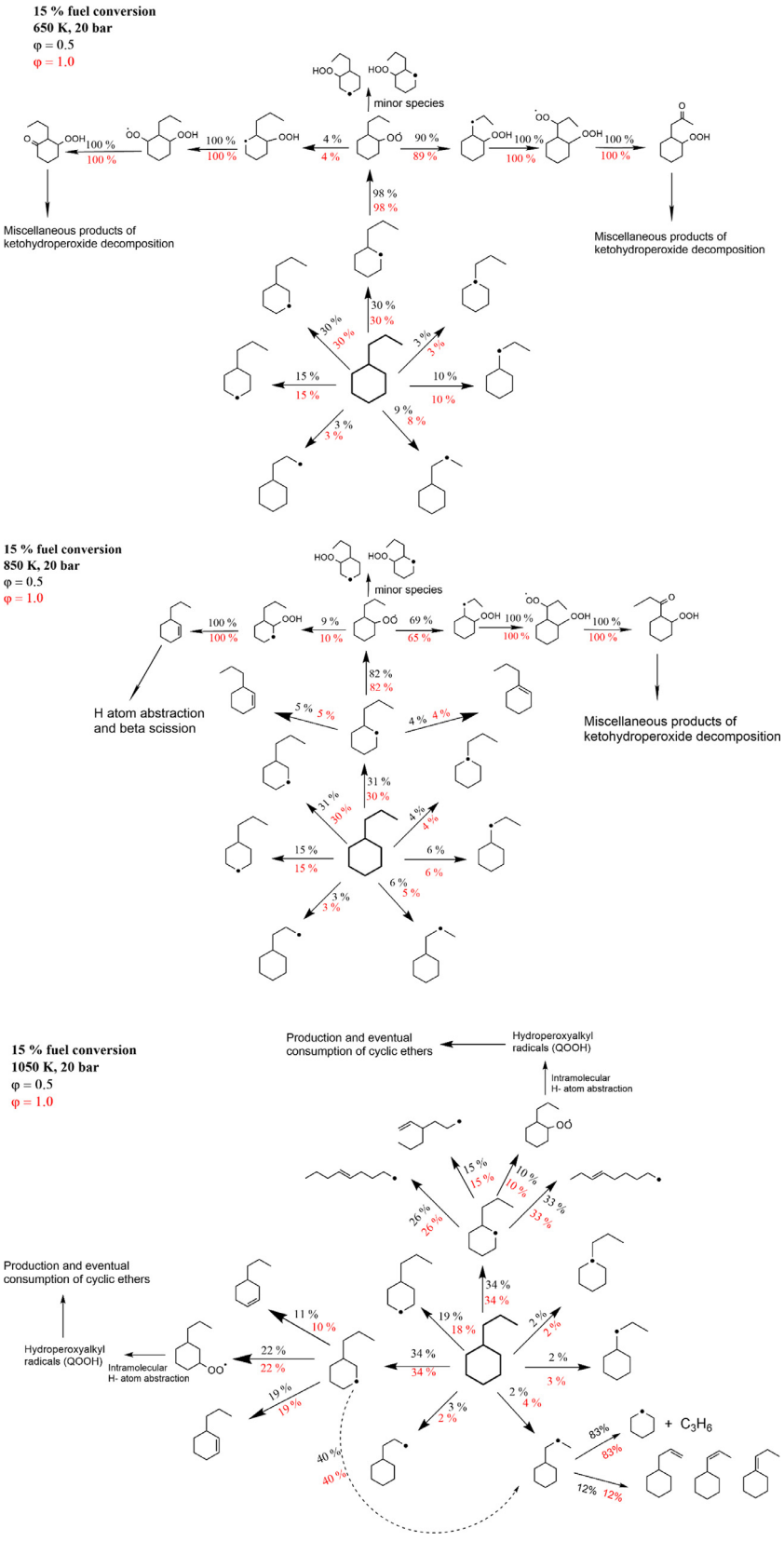

Fig. 19. Dominant fuel consumption pathways of n-Pch at 20 bar, 40 bar at φ = 0.5, 1.0 and 650 K, 850 K and 1050 K.

Table 2
Composition of test mixtures in mole percentages used in JSR measurements.

Species	Equivalence ratios, φ		
	0.5	1.0	2.0
n-Pch	0.005	0.005	0.005
O_2	0.135	0.068	0.034
N_2	0.86	0.928	0.961

tures the trend but over predicts the concentrations by a factor of 5.

During *n*-Pch oxidation, three different aromatic species were measured in minor quantities: benzene, phenol, and ethoxy benzene. A comparison of benzene's computed and experimental values is presented in Fig. 11. Although benzene is produced is insignificant quantities, the proposed kinetic model captures the experimental values.

Lastly, comparisons between computed and experimental values for cyclic alkenes are presented in Fig. 12. Cyclopentene is produced in minor concentrations and is accurately captured by the kinetic model. Similar comparisons for another cycloalkene, cyclohexene, is also presented, and the computed values are slightly higher than the measurements but accurately reproduces the trend.

4.2. Jet stirred reactor: experimental and modelling

The oxidation of *n*-Pch was studied in a JSR at three equivalence ratios, $\varphi = 0.5, 1.0, 2.0$; at atmospheric pressure, and a range of temperatures covering low temperature and NTC region (500–770 K). The initial concentration of the species during the oxidation experiments is provided in Table 2. The concentration profiles of fuel-oxidizer, along with intermediates, is presented in Figs. 13, 14 and 15 for $\varphi = 0.5$, 1.0 and 2.0 respectively. The species measured are carbon monoxide (CO), carbon dioxide (CO_2), ethene (C_2H_4), propene (C_3H_6), *n*-Pch and Oxygen (O_2). At the start of measurement (at 500 K), *n*-Pch is non-reactive at all equivalence ratios. However, with a rise in reactivity increases with increment in equivalence ratio with the mixture being most reactive at $\varphi = 2.0$. At 560 K, CO and CO_2 are first detected and peaks at 620 K coinciding with the start of NTC region. This behavior is consistent with PFR experiments; nevertheless, the start of NTC in PFR is observed at 700 K, resulting from the PFR's leaner equivalence ratio and higher reactor pressure during the experiments. In general, with an increase in pressure the onset of NTC shifts towards higher temperature (i.e., PFR–8 bar and NTC start at 700 K; JSR - 1 bar and NTC start at 620 K) due to the influence of pressure on the chemical equilibrium of molecular oxygen addition to the alkyl and hydroperoxy-alkyl radicals.

The perfectly stirred reactor (PSR) model on Chemkin Pro-ver. 19.2 [78] was used to simulate jet stirred reactor (JSR) experiments conducted in this work. These PSR simulations utilize various experimental details such as species concentrations, reactor geometry, residence time, pressure, and temperature to represent JSR experiments accurately. In line with JSR measurements, computations were conducted at three different equivalence ratios, $\varphi = 0.5$, 1.0, 2.0. Consumption profiles of *n*-Pch, O_2, and evolution profiles for C_2H_4, C_3H_6, CO, CO_2 are compared against experiments and are also presented in Figs. 13,14 and 15 for $\varphi = 0.5$, 1.0, 2.0, respectively. The kinetic model accurately captures the consumption of *n*-Pch in the low-temperature branch until 650 K, however, the model predicts higher reactivity for fuel in the NTC region by ∼ 25% at all three equivalence ratios. The evolution of CO is underpredicted at the fuel-lean condition in the low-temperature region by a factor of ∼1.5. However, the prediction in the NTC region is close to the experimental values. The predicted species profile of CO and CO_2 are closely within the experimental error range. Both the alkenes, ethene and propene were produced in minor quantities during experiments and hence were multiplied by a factor of 10 both in experiments and simulation to improve their visibility. The concentration of ethene was overpredicted while propene was underpredicted by the model.

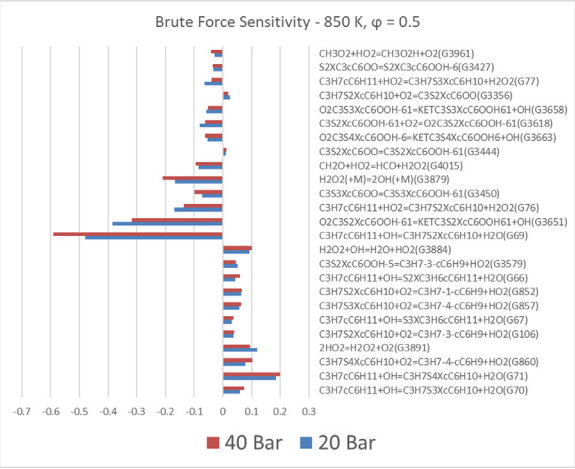

Fig. 20. Sensitivity analysis of n-Pch/air mixture ignition in a shock tube at 20 and 40 bar at $\varphi = 0.5$ and 850 K.

4.3. Shock tube and rapid compression machine: experimental and modelling

Ignition delay measurements have been made in a temperature range of ∼600-1100 K, at pressures of 20 and 40 bar, and two different equivalence ratios $\varphi = 0.5$, 1.0. The measurements at relatively higher temperatures where the ignition delay times are lower than ∼ 10 *ms* are made with the shock tube. The RCM was used at comparatively lower temperatures with longer ignition delay times ($\gtrsim$ 10 *ms*). These ignition delay data and experimental details, including mixture information, are provided in the supplementary material.

Ignition delay data from the shock tube and RCM are presented in Fig. 16 and 17. At both the pressures, ignition delay data shows a weak dependence on equivalence ratio at high and low temperatures. The effect of equivalence ratio was only observed in the NTC region (740–900 K) and the ignition delay times in low and high temperature regions are roughly the same.

Ignition delay simulations for the shock tube (ST) and rapid compression machine (RCM) experiments were carried out using a homogenous batch reactor model in Chemkin Pro-ver. 19.2 [78]. During ST ignition measurements, a pressure rise was observed and was implemented in the ST simulations using an increasing pressure profile at the rate of 3%/ms. Similarly, post-compression heat loss in RCM experiments is represented using inert RCM pressure profiles during these simulations. The comparison of experimental and computed ignition delays is also presented in Fig. 16 and 17 for 20 and 40 bar, respectively. In Fig. 16, the kinetic model captures the RCM experimental ignition delay in the low-temperature range at $\varphi = 1.0$ within a close agreement. However at $\varphi = 0.5$, the RCM measurements span low temperature and the NTC region, and the entire range is very well predicted by the kinetic model with slight over-prediction at 770 K. Shock tube measurements at $\varphi = 0.5$ and 1.0 were slightly overpredicted by the kinetic model.

Shock tube and RCM simulations were also conducted at 40 bar at two equivalence ratios, $\varphi = 0.5$ and 1.0 and were compared to

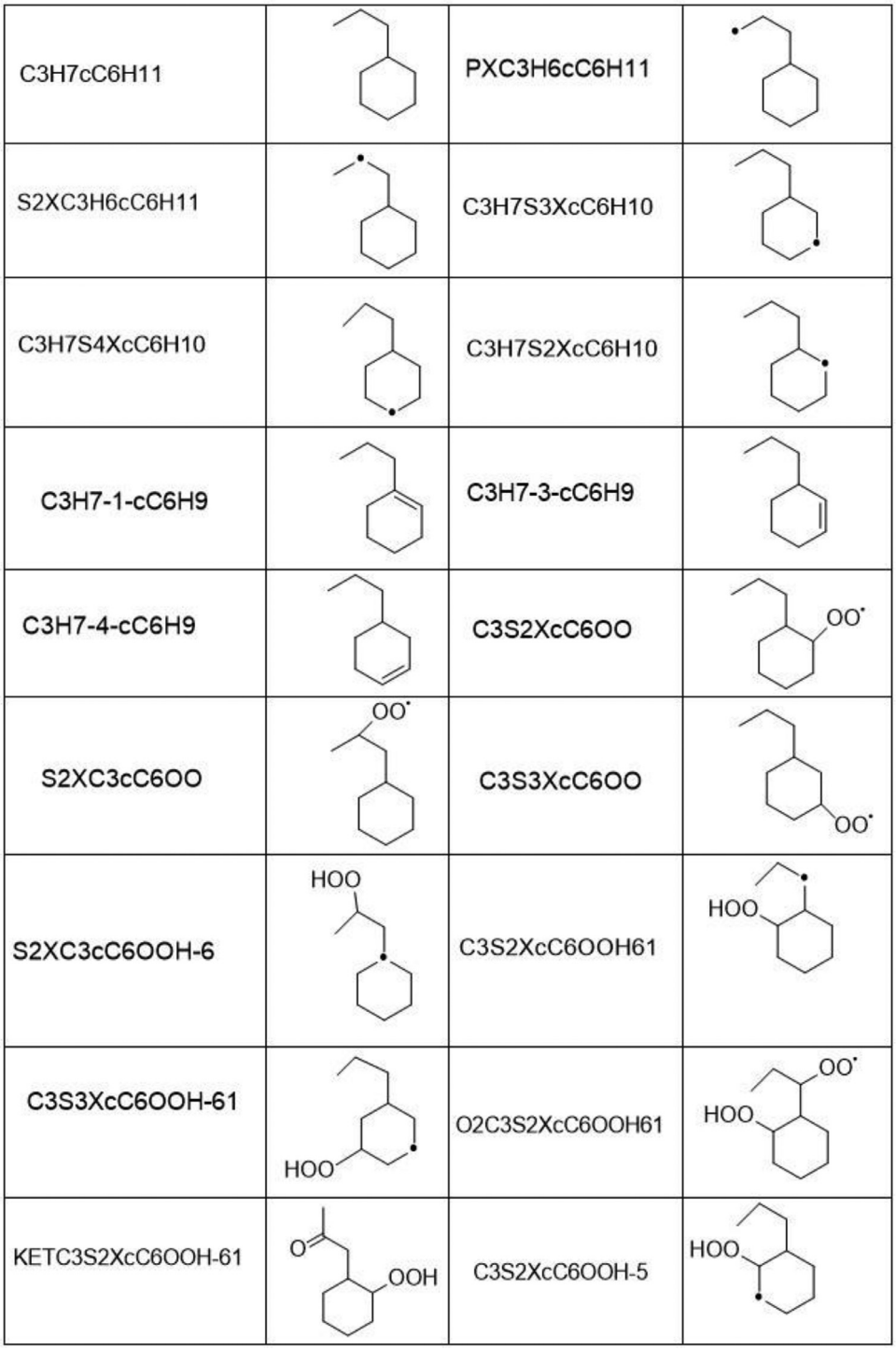

Fig. 21. Species glossary for sensitivity analysis shown in Fig. 20.

the experiment in Fig. 17. The kinetic model well represents the experimental data at low temperature, high temperature and part of the NTC region. The kinetic model to some extent overpredicts the shock tube ignition delay in the high temperature range.

In addition to the data acquired in this study, the developed kinetic model is also compared to ignition delay measurements conducted at 10 bar from Dubois et al. [28] the comparison is presented in Fig. 18. The comparison between the experimental data and the model predictions highlights that the ignition delay predicted by the model is a factor of 2.5 higher over the temperature range at all equivalence ratios. These comparisons also point towards lack of reliable kinetic data for *n*-Pch combustion especially in the high temperature region.

4.4. Chemical kinetic analysis

Flux analysis has been conducted at 20 bar for 650 K, 850 K, 1050 K and $\varphi = 0.5,\ 1.0$ to identify the crucial reactions involved in determining the ignition characteristics of *n*-Pch. These experimental conditions covered the entire range of low, intermediate and high-temperature ignition at two different equivalence ratios.

In addition to the flux analysis, ignition delay sensitivity analysis was also conducted at 20 and 40 bar at $\varphi = 0.5$ and 850 K, where the definition of sensitivity coefficient (S_i) is:

$$S_i = \frac{\left(\tau_{ign(2ki)} - \tau_{ign(ki/2)}\right)}{(2k_i - k_i/2)} \frac{k_i}{\tau_{ign(ki)}}$$

$$S_i = \frac{\left(\tau_{ign(2ki)} - \tau_{ign(ki/2)}\right)}{1.5\tau_{ign(ki)}} \quad (1)$$

where,

$\tau_{ign(2ki)}$ = *ignition delay prediction when ith reaction with rate constant ki is multiplied by* 2

$\tau_{ign(ki/2)}$ = *ignition delay prediction when ith reaction with rate constant ki is divided by* 2

In Fig. 19, the flux analysis of *n*-Pch has been presented at 15% fuel consumption, 20 bar and 650 K, 850 K, 1050 K. At all three temperatures, fuel molecule is predominantly consumed through H-atom abstractions leading to the production of seven fuel radicals. At 650 K, the fuel radicals are further consumed by first O_2 addition, leading to hydroperoxyalkyl radical via internal H atom abstraction from the site adjacent to the ring. Thus, another O_2 molecule is added to the radical site, eventually leading to ketohydroperoxide formation and its eventual decomposition. At 650 K, only pathways are presented for one dominant fuel radical; however, at 650 K being consumed through low-temperature oxidation pathways. Another observation is that the dependence of these pathways on equivalence ratio is minimal as earlier highlighted in Fig. 16 and 17. At 850 K, the fuel molecule undergoes O_2 addition at radical sites to produce RO_2 radicals which further exhibits low-temperature chain branching to eventual production and consumption of ketohydroperoxides. At this temperature RO_2 also exhibits competing pathways to produce cyclic alkenes via QOOH decomposition due to the increase in temperature from 650 K to 850 K.

Eventually, at 1050 K, the low-temperature branching is replaced by β-scission, fuel radical isomerization, cyclic alkene and cyclic ether formation. The fuel radicals thus produced are consumed by β-scission producing cyclic alkenes and alkenyl radicals further consumed by H-atom abstraction and β-scission. The H-atom abstraction reaction's dominant products are R5, R6 and R7 (in Fig. 2), which are also the most significant pathway as identified in the sensitivity analysis in Fig. 20. The sensitivity analysis identifies reactions playing a significant role in determining ignition delay time or reactivity of the system at these conditions. As per Eqn. (1) and an increase in the magnitude of the A-factor of the reactions with sensitivity coefficient in positive directions will inhibit the reactivity of the system by increasing the ignition delay; while increasing the A-factor of reactions with negative sensitivity coefficients will promote reactivity, thus decreasing the ignition delay time. In Fig. 20, apart from G69, there are some other notable reactions such as decomposition of hydroperoxide (H_2O_2) to two hydroxyl radicals (OH) (G3879) and formation of ketohydroperoxide from peroxyhydroperoxyalkyl radical (G3651). While decomposition of H_2O_2 is a significant source of hydroxyl radicals controlling the ignition process, the formation and eventual decomposition of ketohydroperoxides also promotes ignition by releasing hydroxyl radicals. At 40 bar, higher yield of fuel radical $C_3H_7S_2XcC_6H_{10}$ is observed as shown in Fig. 20 which further leads to the production of higher concentrations of intermediates in the low-temperature chain branching process including production and decomposition of ketohydroperoxides. This higher branching ratio leads to increased reactivity at 40 bar, which results in lower ignition delay and suppressed NTC behavior. Another explanation of this shift in NTC behavior could be derived from the method of experimental measurements. The structure of species discussed in the sensitivity analysis in Fig. 20 is depicted in Fig. 21.

5. Summary and conclusion

This work presents a detailed experimental, kinetic modelling and quantum chemistry study of *n*-propylcyclohexane, a crucial component of jet fuels. The oxidation of *n*-propylcyclohexane was studied experimentally using several experiments including jet stirred reactor (JSR), pressurized flow reactor (PFR), shock tube (ST) and rapid compression machine (RCM) covering a wide range of pressure, temperature and equivalence ratios. Further, a detailed chemical kinetic model comprising of low, intermediate and high-temperature kinetics was developed. The reaction rates for *n-propylcyclohexane* consumption were estimated based on analogies with existing and analogous species mechanisms. The thermochemistry for several new species was also estimated by quantum chemistry methods and group additivity approach. The kinetic model predictions were compared against the experimental data with satisfactory agreements for speciation data from the JSR and PFR measurements for several major species. There is room for improving the kinetic model for several minor intermediates measured in these experiments. Experimental and simulated ignition delays were also compared. The model satisfactorily describes the ignition characteristics of *n*-propylcyclohexane in the entire region with exception of longer predicted ignition delay time in high-temperature and in the NTC region. The model was also compared with experimental ignition delay data at 10 bar from Dubois et al.[28]. and the model was found to over predict the ignition delay times at all equivalence ratios, highlighting the need for calculations and measurements of reliable reaction rates describing *n-p*ropylcyclohexane kinetics.

This work provides a comprehensive investigation of *n*-propylcyclohexane combustion chemistry and will prove instrumental in studies of analogous alkylated cyclic alkanes.

Declaration of Competing Interest

The authors declare that they have no known competing financial interests or personal relationships that could have appeared to influence the work reported in this paper.

Acknowledgements

The work at King Abdullah University of Science and Technology (KAUST) was supported by the KAUST Clean Fuels Consortium (KCFC) and its member companies.

The investigations at Drexel University were based upon work supported by the US Air Force Office of Scientific Research under Grant No. FA9550–08–1–0040 (AFRL Energy IPT – Phase I) and Grant No. FA9550–11–1–0217 (AFRL Energy IPT – Phase II), and by Drexel University.

Supplementary materials

Supplementary material associated with this article can be found, in the online version, at doi:10.1016/j.combustflame.2021.111576.

References

[1] J. Timperley, Corsia: The UN's plan to 'offset' growth in aviation emissions after 2020. https://www.carbonbrief.org/corsia-un-plan-to-offset-growth-in-aviation-emissions-after-2020 (accessed 10 Aug 2019). 2019.

[2] Y. Alexandrov, V. Sychenkov, R. Khaliulin, W. Yousef, S. Semichev, Optimization and improvement of the gas turbine engine exhaust based on hydraulic and acoustic characteristics, Int. Conf. Dyn. Vibroacous. Machines (DVM), IEEE (2020), pp. 1–7.

[3] F.C. Barbosa, Aircraft Engine Technology Review-The Pathways for an Efficient, Cleaner and Quieter Aviation Industry, SAE Technical Paper 0148-7191, 2020.

[4] Z. Xu, F. Ji, S. Ding, Y. Zhao, X. Zhang, Y. Zhou, Q. Zhang, F. Du, High-altitude performance and improvement methods of poppet valves 2-stroke aircraft diesel engine, Appl. Energy 276 (2020) 115471.

[5] A. Anderson, A. Karthikeyan, S. Ramachandran, T.Praveen Kumar, Lowest emission sustainable aviation biofuels as the potential replacement for the Jet-A fuels, Aircraft Eng. Aero. Technol. (2020) AEAT-07-2020-0135.

[6] M.A. Mayorga, M. Lopez, C. Lopez, J. Bonilla, V. Silva, G. Talero, F. Correa, M. Noriega, Production of aviation biofuel from palm Kernel Oil, Chem. Eng. Trans. 80 (2020) 319–324.

[7] L. Shafer, R. Striebich, J. Gomach, T. Edwards, Chemical class composition of commercial jet fuels and other specialty kerosene fuels, 14th AIAA, 2012.

[8] D. Han, J. Zhai, Z. Huang, Autoignition of n-Hexane, Cyclohexane, and Methylcyclohexane in a Constant Volume Combustion Chamber, Energy Fuels 33 (2019) 3576–3583.

[9] Z. Hong, K.-Y. Lam, D.F. Davidson, R.K. Hanson, A comparative study of the oxidation characteristics of cyclohexane, methylcyclohexane, and n-butylcyclohexane at high temperatures, Combust. Flame 158 (2011) 1456–1468.

[10] W.J. Pitz, C. Naik, T.N. Mhaoldúin, C.K. Westbrook, H.J. Curran, J.P. Orme, J. Simmie, Modeling and experimental investigation of methylcyclohexane ignition in a rapid compression machine, Proc. Combust. Inst. 31 (2007) 267–275.

[11] J. Vanderover, M.A. Oehlschlaeger, Ignition time measurements for methylcyclohexane and ethylcyclohexane-air mixtures at elevated pressures, Int. J. Chem. Kin. 41 (2009) 82–91.

[12] S.S. Vasu, D.F. Davidson, Z. Hong, R.K. Hanson, Shock tube study of methylcyclohexane ignition over a wide range of pressure and temperature, Energy Fuels 23 (2008) 175–185.

[13] B.W. Weber, W.J. Pitz, M. Mehl, E.J. Silke, A.C. Davis, C.-J. Sung, Experiments and modeling of the autoignition of methylcyclohexane at high pressure, Combust. Flame 161 (2014) 1972–1983.

[14] S. Humer, A. Frassoldati, S. Granata, T. Faravelli, E. Ranzi, R. Seiser, K. Seshadri, Experimental and kinetic modeling study of combustion of JP-8, its surrogates and reference components in laminar nonpremixed flows, Proc. Combust. Inst. 31 (2007) 393–400.

[15] T. Bissoonauth, Z. Wang, S.Y. Mohamed, J.-y. Wang, B. Chen, A. Rodriguez, O. Frottier, X. Zhang, Y. Zhang, C. Cao, Methylcyclohexane pyrolysis and oxidation in a jet-stirred reactor, Proc. Combust. Inst. 37 (2019) 409–417.

[16] K. Narayanaswamy, H. Pitsch, P. Pepiot, A chemical mechanism for low to high temperature oxidation of methylcyclohexane as a component of transportation fuel surrogates, Combust. Flame 162 (2015) 1193–1213.

[17] Y. Yang, A.L. Boehman, Experimental study of cyclohexane and methylcyclohexane oxidation at low to intermediate temperature in a motored engine, Proc. Combust. Inst. 32 (2009) 419–426.

[18] Z. Wang, L. Ye, W. Yuan, L. Zhang, Y. Wang, Z. Cheng, F. Zhang, F. Qi, Experimental and kinetic modeling study on methylcyclohexane pyrolysis and combustion, Combust. Flame 161 (2014) 84–100.

[19] J.P. Orme, H.J. Curran, J.M. Simmie, Experimental and modeling study of methyl cyclohexane pyrolysis and oxidation, J. Phys. Chem. A 110 (2006) 114–131.

[20] H. Wang, E. Dames, B. Sirjean, D.A. Sheen, R. Tango, A. Violi, J.Y.W. Lai,F.N. Egolfopoulos, D.F. Davidson, R.K. Hanson, C.T. Bowman, C.K. Law, W. Tsang, N.P. Cernansky, D.L. Miller, R.P. Lindstedt, A high-temperature chemical kinetic model of n-alkane (up to n-dodecane), cyclohexane, and methyl-, ethyl-, n-propyl and n-butyl-cyclohexane oxidation at high temperatures, http://web.stanford.edu/group/haiwanglab/JetSurF/JetSurF2.0/index.html, 2010.

[21] F. Wu, A.P. Kelley, C.K. Law, Laminar flame speeds of cyclohexane and mono-alkylated cyclohexanes at elevated pressures, Combust. Flame 159 (2012) 1417–1425.

[22] B. Husson, O. Herbinet, P.A. Glaude, S.S. Ahmed, F. Battin-Leclerc, Detailed product analysis during low-and intermediate-temperature oxidation of ethylcyclohexane, J. Phys. Chem. A 116 (2012) 5100–5111.

[23] Z. Tian, Y. Zhang, F. Yang, L. Pan, X. Jiang, Z. Huang, Comparative study of experimental and modeling autoignition of cyclohexane, ethylcyclohexane, and n-propylcyclohexane, Energy Fuels 28 (2014) 7159–7167.

[24] Z. Tian, Y. Zhang, L. Pan, J. Zhang, F. Yang, X. Jiang, Z. Huang, Shock-tube study on ethylcyclohexane ignition, Energy Fuels 28 (2014) 5505–5514.

[25] Z. Wang, H. Bian, Y. Wang, L. Zhang, Y. Li, F. Zhang, F. Qi, Investigation on primary decomposition of ethylcyclohexane at atmospheric pressure, Proc. Combust. Inst. 35 (2015) 367–375.

[26] Z. Wang, L. Zhao, Y. Wang, H. Bian, L. Zhang, F. Zhang, Y. Li, S.M. Sarathy, F. Qi, Kinetics of ethylcyclohexane pyrolysis and oxidation: an experimental and detailed kinetic modeling study, Combust. Flame 162 (2015) 2873–2892.

[27] M. Crochet, R. Minetti, M. Ribaucour, G. Vanhove, A detailed experimental study of n-propylcyclohexane autoignition in lean conditions, Combust. Flame 157 (2010) 2078–2085.

[28] T. Dubois, N. Chaumeix, C.-E. Paillard, Experimental and modeling study of n-propylcyclohexane oxidation under engine-relevant conditions, Energy Fuels 23 (2009) 2453–2466.

[29] J. Guo, J. Wang, X. Hua, Z. Li, N. Tan, X. Li, Mechanism construction and simulation for high-temperature combustion of n-propylcyclohexane, Chem. Res. Chin. Uni. 30 (2014) 480–488.

[30] A. Ristori, P. Dagaut, A.E. Bakali, M. Cathonnet, The oxidation of n-propylcyclohexane: experimental results and kinetic modeling, Combust. Sci. Techno. 165 (2001) 197–228.

[31] F. Farid, J. Corrubia, N. Cernansky, D. Miller, Oxidation of 2, 7-Dimethyloctane and n-Propylcyclohexane in the Low to Intermediate Temperature Regime with a Pressurized Flow Reactor, 8th U.S. Natnl. Combust. Meet., University of Utah, 2013.

[32] J. Corrubia, F. Farid, N. Cernansky, D. Miller, The Low to Intermediate Temperature Oxidation of n Propylcyclohexane in a Pressurized Flow Reactor, Drexel University Philadelphia, USA. College of Engineering, 2011 Research day posters.

[33] J.A. Corrubia, Low Temperature Oxidation of N-Propylcyclohexane in a Pressurized Flow Reactor, Drexel University, Philadelphia, USA, 2018 PhD Thesis.

[34] E. Pousse, R. Porter, V. Warth, P.A. Glaude, R. Fournet, F. Battin-Leclerc, Lean methane premixed laminar flames doped by components of diesel fuel II: n-Propylcyclohexane, Combust. Flame 157 (2010) 75–90.

[35] C. Conroy, A High-Pressure Shock Tube and Rapid Compression Machine Study of N-Butylcyclohexane and Its Mixtures with N-Heptane, National University of Ireland, Galway, 2013 PhD Thesis.

[36] Y. Mao, S. Wang, Z. Wu, Y. Qiu, L. Yu, C. Ruan, F. Chen, L. Zhu, X. Lu, An experimental and kinetic modeling study of n-butylcyclohexane over low-to-high temperature ranges, Combust. Flame 206 (2019) 83–97.

[37] R.H. Natelson, Oxidation of N-Butylcyclohexane in the Low Temperature Region, Drexel University Philadelphia, USA, 2010 PhD Thesis.

[38] R.H. Natelson, M.S. Kurman, N.P. Cernansky, D.L. Miller, Low temperature oxidation of n-butylcyclohexane, Combust. Flame 158 (2011) 2325–2337.

[39] W. Pitz, C. Conroy, J. Bugler, H. Curran, An Experimental and Modeling Study of the Autoignition of N-Butylcyclohexane Over a Wide Pressure, Temperature and Equivalence-Ratio Range, Lawrence Livermore National Lab.(LLNL, Livermore, CA (United States), 2015.

[40] S.M. Sarathy, C.K. Westbrook, M. Mehl, W.J. Pitz, C. Togbe, P. Dagaut, H. Wang, M.A. Oehlschlaeger, U. Niemann, K. Seshadri, Comprehensive chemical kinetic modeling of the oxidation of 2-methylalkanes from C7 to C20, Combust. Flame 158 (2011) 2338–2357.

[41] D. Zhang, Y. Wang, Z. Wan, P. Li, C. Zhang, Study of n-Butylcyclohexane/Air Ignition over a Broad Range of Temperatures in Shock Tube, Combust. Sci. Techno. (2019) 1–13.

[42] Y. Mao, A. Li, L. Zhu, Z. Wu, L. Yu, S. Wang, M. Raza, X. Lu, A detailed chemical mechanism for low to high temperature oxidation of n-butylcyclohexane and its validation, Combust. Flame 210 (2019) 360–373.

[43] M. Akbar Ali, V.T. Dillstrom, J.Y. Lai, A. Violi, Ab initio investigation of the thermal decomposition of n-butylcyclohexane, J. Phys. Chem. A 118 (2014) 1067–1076.

[44] N. Liu, C. Ji, F.N. Egolfopoulos, Ignition of non-premixed cyclohexane and mono-alkylated cyclohexane flames, Proc. Combust. Inst. 34 (2013) 873–880.

[45] Y. Li, C.-W. Zhou, K.P. Somers, K. Zhang, H.J. Curran, The oxidation of 2-butene: a high pressure ignition delay, kinetic modeling study and reactivity comparison with isobutene and 1-butene, Proc. Combust. Inst. 36 (2017) 403–411.

[46] F. Zhang, Z. Wang, Z. Wang, L. Zhang, Y. Li, F. Qi, Kinetics of decomposition and isomerization of methylcyclohexane: starting point for studying monoalkylated cyclohexanes combustion, Energy Fuels 27 (2013) 1679–1687.

[47] M.A. Oehlschlaeger, D.F. Davidson, R.K. Hanson, High-temperature thermal decomposition of Isobutane and n-Butane Behind Shock Waves, J. Phys. Chem. A 108 (2004) 4247–4253.

[48] J. Badra, A. Elwardany, A. Farooq, Shock tube measurements of the rate constants for seven large alkanes+OH, Proc. Combust. Inst. 35 (2015) 189–196.

[49] Y.-X. Liu, B.-Y. Wang, J.-J. Weng, D. Yu, S. Richter, T. Kick, C. Naumann, M. Braun-Unkhoff, Z.-Y. Tian, A wide-range experimental and modeling study of oxidation and combustion of n-propylbenzene, Combust. Flame 191 (2018) 53–65.

[50] Z. Wang, L. Zhao, Y. Wang, H. Bian, L. Zhang, F. Zhang, Y. Li, S.M. Sarathy, F. Qi, Kinetics of ethylcyclohexane pyrolysis and oxidation: an experimental and detailed kinetic modeling study, Combust. Flame 162 (2015) 2873–2892.

[51] H.J. Curran, P. Gaffuri, W.J. Pitz, C.K. Westbrook, A comprehensive modeling study of iso-octane oxidation, Combust. Flame 129 (2002) 253–280.

[52] T.M. Lenhardt, C.E. McDade, K.D. Bayes, Rates of reaction of butyl radicals with molecular oxygen, J. Chem. Phys. 72 (1980) 304–310.

[53] R. Atkinson, D.L. Baulch, R.A. Cox, R.F.H. Jr., J.A. Kerr, M.J. Rossi, J. Troe, Evaluated kinetic, photochemical and heterogeneous data for atmospheric chemistry: supplement V. IUPAC subcommittee on gas kinetic data evaluation for atmospheric chemistry, J. Phys. Chem. Ref. Data 26 (1997) 521–1011.

[54] R.X. Fernandes, J. Zádor, L.E. Jusinski, J.A. Miller, C.A. Taatjes, Formally direct pathways and low-temperature chain branching in hydrocarbon autoignition: the cyclohexyl+ O2 reaction at high pressure, Phys. Chem. Chem. Phys. 11 (2009) 1320–1327.

[55] Z. Wang, S.M. Sarathy, Third O2 addition reactions promote the low-temperature auto-ignition of n-alkanes, Combust. Flame 165 (2016) 364–372.

[56] N. Hansen, G. Kukkadapu, B. Chen, S. Dong, H. Curran, C. Taatjes, A. Eskola, D. Osborn, L. Sheps, W. Pitz, The impact of the third O2 addition reaction network on ignition delay times of neo-pentane, Proc. Combust. Inst. 38 (1) (2020) 299–307.

[57] H.J. Curran, P. Gaffuri, W.J. Pitz, C.K. Westbrook, A comprehensive modeling study of n-Heptane Oxidation, Combust. Flame 114 (1998) 149–177.

[58] D. Darcy, M. Mehl, J.M. Simmie, J. Würmel, W.K. Metcalfe, C.K. Westbrook, W.J. Pitz, H.J. Curran, An experimental and modeling study of the shock tube

ignition of a mixture of n-heptane and n-propylbenzene as a surrogate for a large alkyl benzene, Proc. Combust. Inst. 34 (1) (2013) 411–418.
[59] M.J. Frisch, G.W. Trucks, H.B. Schlegel, G.E. Scuseria, M.A. Robb, J.R. Cheeseman, G. Scalmani, V. Barone, G.A. Petersson, H. Nakatsuji, X. Li, M. Caricato, A.V. Marenich, J. Bloino, B.G. Janesko, R. Gomperts, B. Mennucci, H.P. Hratchian, J.V. Ortiz, A.F. Izmaylov, J.L. Sonnenberg, F. Williams, F. Ding, F. Lipparini, J. Egidi, B. Goings, A. Peng, T. Petrone, D. Henderson, V.G. Ranasinghe, J. Zakrzewski, N. Gao, G. Rega, W. Zheng, M. Liang, M. Hada, K. Ehara, R. Toyota, J. Fukuda, M. Hasegawa, T. Ishida, Y. Nakajima, O. Honda, H. Kitao, T. Nakai, K. Vreven, J.A. Throssell, Montgomery Jr., J.E. Peralta, F. Ogliaro, M.J. Bearpark, J.J. Heyd, E.N. Brothers, K.N. Kudin, V.N. Staroverov, T.A. Keith, R. Kobayashi, J. Normand, K. Raghavachari, A.P. Rendell, J.C. Burant, S.S. Iyengar, J. Tomasi, M. Cossi, J.M. Millam, M. Klene, C. Adamo, R. Cammi, J.W. Ochterski, R.L. Martin, K. Morokuma, O. Farkas, J.B. Foresman, D.J. Fox, Gaussian 16 Rev. A.03, Wallingford, CT, 2016.
[60] A.D. Becke, Density-functional thermochemistry. III. the role of exact exchange, J. Chem. Phys. 98 (1993) 5648–5652.
[61] C. Lee, W. Yang, R.G. Parr, Development of the Colle-Salvetti correlation-energy formula into a functional of the electron density, Phys. Rev. B 37 (1988) 785.
[62] J.A. Montgomery Jr, M.J. Frisch, J.W. Ochterski, G.A. Petersson, A complete basis set model chemistry. VII. Use of the minimum population localization method, J. Chem. Phys. 112 (2000) 6532–6542.
[63] C. Sheng, Elementary, Pressure Dependent Model For Combustion of C1, C2 and Nitrogen Containing hydrocarbons: Operation of a Pilot Scale Incinerator and Model Comparison, New Jersey Institute of Technology, Newark USA, 2001 PhD Thesis.
[64] R.D. Johnson III, NIST computational chemistry comparison and benchmark database, NIST Standard Reference Database Number 101, NIST, 2010.
[65] T.H. Lay, L.N. Krasnoperov, C.A. Venanzi, J.W. Bozzelli, N.V. Shokhirev, Ab initio study of α-chlorinated ethyl hydroperoxides CH3CH2OOH, CH3CHClOOH, and CH3CCl2OOH: conformational analysis, internal rotation barriers, vibrational frequencies, and thermodynamic properties, J. Phys. Chem. 100 (1996) 8240–8249.
[66] S.W. Benson, Thermochemical kinetics: Methods For the Estimation of Thermochemical Data and Rate Parameters, Wiley, 1968.
[67] E.R. Ritter, THERM: a computer code for estimating thermodynamic properties for species important to combustion and reaction modeling, J. Chem. Info. Comp. Sci. 31 (1991) 400–408.
[68] CloudflameKAUST Thuwal, Saudi Arabia, 2018.
[69] D.N. Koert, Effects of Pressure On Hydrocarbon Oxidation Chemistry, Drexel University, Philadelphia, USA, 1990 PhD Thesis.
[70] M.S. Kurman, The Preignition Oxidation Chemistry of N-Decane and N-Dodecane in a Pressurized Flow Reactor and Their Use As Jet Fuel Surrogate Components, Drexel University, Philadelphia, USA, 2010 PhD Thesis.
[71] M. Kurman, R. Natelson, N. Cernansky, D. Miller, New methodology for jet fuel surrogate oxidation and intermediate speciation in the low temperature regime, 6th US Natnl. Combust. Meet, Paper No. USSCI-09-23G2, University of Michigan, 2009.
[72] O. Herbinet, B. Husson, Z. Serinyel, M. Cord, V. Warth, R. Fournet, P.-.A. Glaude, B. Sirjean, F. Battin-Leclerc, Z. Wang, Experimental and modeling investigation of the low-temperature oxidation of n-heptane, Combust. Flame 159 (2012) 3455–3471.
[73] B. Chen, Gasoline Combustion Chemistry in a Jet Stirred Reactor, KAUST, Saudi Arabia, 2019 PhD Thesis.
[74] T. Javed, E.F. Nasir, A. Ahmed, J. Badra, K. Djebbi, M. Beshir, W. Ji, S.M. Sarathy, A. Farooq, Ignition delay measurements of light naphtha: a fully blended low octane fuel, Proc. Combust. Inst. 36 (2017) 315–322.
[75] E.F. Nasir, A. Farooq, Time-resolved temperature measurements in a rapid compression machine using quantum cascade laser absorption in the intrapulse mode, Proc. Combust. Inst. 36 (2017) 4453–4460.
[76] R. Wilk, D. Koert, N. Cernansky, Low-temperature carbon monoxide formation as a means of assessing the autoignition tendency of hydrocarbons and hydrocarbon blends, Energy Fuels 3 (1989) 292–298.
[77] M.S. Kurman, R.H. Natelson, N.P. Cernansky, D.L. Miller, Speciation of the reaction intermediates from n-dodecane oxidation in the low temperature regime, Proc. Combust. Inst. 33 (2011) 159–166.
[78] ANSYS Reaction Design: Chemkin Pro 19.2, San Diego, 2019.